Exploiting Hierarchical Features for Crop Yield Prediction Based on 3-D Convolutional Neural Networks and Multikernel Gaussian Process

Mengjia Qiao, Xiaohui He, Xijie Cheng, Panle Li, Haotian Luo, Zhihui Tian, and Hengliang Guo

***Abstract*—Accurate and timely prediction of crop yield based on remote sensing data is important for food security. However, crop growth is a complex process, which makes it quite difficult to achieve better performance. To address this problem, a novel 3-D convolutional neural multikernel network is proposed to capture hierarchical features for predicting crop yield. First, a full 3-D convolutional neural network is constructed to maximally explore deep spatial–spectral features from multispectral images. Then, a multikernel learning (MKL) approach is proposed for fusion of intraimage deep spatial–spectral features and intersample spatial consistency features. Specifically, we assign a group of nonlinear kernels for each feature in the MKL framework, which provides a robust way to fit features extracted from different domains. Finally, the probability distribution of prediction results is obtained by a kernel-based method. We evaluate the performance of the proposed method on China wheat yield prediction and offer detailed and systematic analyses of the performance of the proposed method. In addition, our method is compared with several competing methods. Experimental results demonstrate that the proposed method has certain advantages and can provide better prediction performance than the competitive methods.**

***Index Terms*—Crop yield, multikernel learning (MKL), spatial consistency, 3-D convolutional neural network (CNN).**

I. Introduction

CROP yield prediction is an essential and active part of improving food security. A reliable and timely estimation of crop yield before harvest is of great significance and has been a topic of interest for decades. Traditionally, researchers focused on predicting crop yields through crop simulation models (CSMs) [1], [2]. Two main dilemmas arise in adopting CSMs in crop yield prediction. First, a substantial number of indicators are needed for model calibration that restrict these models from broad applications. Second, CSMs are commonly designed for specific regions based on the situations of current interest, which makes it difficult to accurately estimate yields in other regions. To overcome these drawbacks, later studies cast yield prediction problems from the perspective of machine learning methods, such as support vector machines (SVM) [3], [4], random forests (RF) [5], [6], artificial neural networks (ANN) [7]–[9], etc. These algorithms can build empirical predictive models using a fixed pattern of features extracted from remote sensing images (RSIs) without abundant parameters. However, the performance is still limited because handcrafted features mainly leverage human ingenuity and prior knowledge [10], which are not robust for all cases. Furthermore, such algorithms are computationally intensive and become intractable on large-scale datasets. All such difficulties make crop yield prediction challenging and lead to unsatisfactory performance.

With the development of deep learning methods, an important trend in crop yield prediction is the use of deep models. Compared with traditional approaches, these models can automatically extract informative features from the raw image, which enable generalization for coping with different situations [11], [12]. Ma *et al.* [13] introduced a stacked autoencoder (SAE) to extract the deep spectral features for crop yield prediction using multispectral images (MSIs). However, this method flattens images into 1-D spectral vectors that suffer from spatial information loss. To address this issue, the authors of [14]–[17] proposed the use of convolutional neural networks (CNNs) for crop yield prediction. Compared with SAEs, CNNs allow using spatial patches as input that provide a natural way to incorporate spatial information and enhance the performance [18]. Moreover, Yang *et al.* [19] developed a two-branch CNN to separately extract spectral and spatial features. These methods have achieved better results than traditional approaches and have proven that the deep spatial and spectral features excavated by CNNs can create a generalized representation for crop yield prediction.

However, in the real world, crop growth is a highly complex trait determined by many factors such as soil properties, precipitation, etc., which are not fully captured by RSIs. In such cases, merely excavating intraimage deep spatial and spectral features based on CNNs may be insufficient. It has been observed that these crop-related factors have a strong consistency trend in the spatial dimension [20], [21]. In this scenario, the use of this spatial consistency between different data points could be of help to incorporate properties of other missing factors into the task of prediction. As demonstrated by Anselin *et al.* [22], spatial correlation was prevalent in corn yield response models and should be critically considered in the analysis of yield

Manuscript received September 24, 2020; revised March 20, 2021; accepted April 9, 2021. Date of publication April 14, 2021; date of current version May 12, 2021. This work was supported by the National Key Research and Development Program of China under Grant 2018YFB0505000. *(Corresponding author: Xiaohui He.)*

Mengjia Qiao, Xijie Cheng, and Panle Li are with the School of Information Engineering, Zhengzhou University, Zhengzhou 450001, China (e-mail: qiaomjj@163.com; 465097566@qq.com; 13137052075@163.com).

Xiaohui He, Haotian Luo, Zhihui Tian, and Hengliang Guo are with the School of Geoscience and Technology, Zhengzhou University, Zhengzhou 450001, China (e-mail: hexh@zzu.edu.cn; lht1321201105@163.com; iezhtian@zzu.edu.cn; guohengliang@zzu.edu.cn).

Digital Object Identifier 10.1109/JSTARS.2021.3073149

monitor data. Peralta *et al.* [23] pointed that without accounting for spatial consistency, prediction models may lead to inaccurate estimations. Following these rationales, the spatial consistency property has been intensively incorporated in rice [24], grain [20], and soybean [21] prediction and achieved improved performance. Hence, we assume that the integrated use of deep spatial–spectral features and spatial consistency can help as an ensemble of multiple crop-related characters for predicting crop yield, which would effectively improve the results. Nevertheless, since these two features are typically obtained from different sources, determining how to simultaneously integrate these two heterogeneous levels of information into the prediction model is a substantial challenge. To overcome this problem, we propose a multikernel learning (MKL) approach associated with a kernel-based Gaussian process (GP) for integrating heterogeneous features as well as a feature selection strategy for inferring the contribution of each feature.

In this article, we aim at fully exploiting and utilizing the discriminative power of hierarchical features for crop yield prediction. Based on this intention, we propose a novel architecture (3DMKGP) for crop yield prediction, which is a combination of the 3-D CNN and the multikernel GP (MKGP). Although the 3-D CNN has been used for crop yield prediction in earlier works [25], [26], to the best of our knowledge, we are first to apply it for excavating the joint spatial–spectral features from MSIs. Note that the GP has been explored in [14], where a linear GP is utilized for final prediction and the spatial consistency is only taken as the residual of the prediction. In our work, a novel MKL strategy is not only employed for seamlessly generalizing deep features and spatial consistency within a kernel function, but is also used for measuring the uncertainty of the predictions. The main contributions of this article are listed as follows.

1) A 3-D CNN is first applied for excavating spatial–spectral features in the crop yield prediction assessment. By applying 3-D convolutions, the robust spatial–spectral features can be simultaneously extracted.
2) An MKGP with a new "spatial–spectral–spatio" composite Gaussian kernel is concatenated on the top of the 3-D CNN. The new kernel is derived from deep features and location data and can flexibly encode deep feature characteristics and spatial consistency.
3) County-level wheat yield in China is predicted to show the effectiveness of the proposed method. Experimental results show that our method achieves a promising modeling capability and is capable of predicting crop yield with higher quality.

The rest of this article is organized as follows. Section II presents an introduction of crop yield prediction and MKL. Section III describes the proposed 3DMKGP in detail. Section IV then provides the dataset information and experimental results. Finally, Section V concludes this article.

II. Related Works

A. Traditional-Based Methods for Crop Yield Prediction

Crop yield prediction has been a vital problem for decades, and many methods have been proposed to forecast crop yields. The most commonly used approach for prediction yield is crop yield models. Generally, we can classify all previous crop yield models into two categories. The models in the first category forecast crop yields by simulating multiple physiological characteristics of crops, such as meteorological data, soil properties, biogeochemical fluxes, relevant socioeconomic indicators, etc. The most widely used models include AquaCrop [27], the CERES-Maize model [28], and the APSIM model [29]. However, these kinds of models require a massive number of indicators as input, which are hard to obtain, especially in developing counties. Furthermore, these models exhibit weak spatial generalization, which limits these models from wider application. The second category is the machine-learning-based models. These kinds of models are based on handcrafted features, such as the normalized difference vegetation index (NDVI) and the enhanced vegetation index (EVI). A considerable body of work in the crop yield prediction community falls into this category. For example, in [30], the NDVI and the EVI from MODIS were used to establish an empirical approach to forecast maize yield in the USA. Moreover, Vega *et al.* [31] also demonstrated good correlation between sunflower yield and the calculated NDVI from pixel-based MSIs based on an SVM. Similar studies evaluated different methods for various crop types, e.g., regression trees for wheat [32] and corn [33], multilinear regression for barely [34] and rice prediction [35], and so on. After that, in order to incorporate more complex modeling problems, Bose *et al.* [9] later introduced spiking neural networks for crop yield estimation from NDVI image time series, which have been shown to outperform traditional machine learning classifiers. However, these traditional machine-learning-based methods are still limited by handcrafted features, since they are mostly mathematical combinations of a few fixed bands and are not robust for all cases [36].

B. Deep-Learning-Based Methods for Crop Yield Prediction

Recently, deep learning methods have shown great potential in the field of urban planning [37], [38], land cover classification [39], [40], and gradually developed in crop yield prediction. Compared to traditional approaches, the deep learning methods can automatically extract robust features from the original image using a hierarchical representation architecture. Peerlinck *et al.* [41] introduced an SAE to extract high-level features for crop yield prediction based on MSIs. In this work, the images were flattened into a 1-D spectral vector that could not exploit the spatial information. To overcome this limitation, You *et al.* [14] first introduced a CNN and a long short-term memory (LSTM) network to automatically discover crop-related features from raw images for crop yield prediction in America, and the results showed that both the CNN and the LSTM achieve better results than the traditional approach. Compared to the SAE, the CNN can preserve local spatial information from spatial patches through 2-D convolution filters. Based on this intention, many research works have applied CNNs to the task of excavating spatial and spectral features in crop yield prediction [15], [42]. Moreover, the authors of [16] and [17] provided an extension to new regions with a transfer learning approach, which further

exhibited the superiority of deep learning methods in extracting spatial and spectral features. More recently, Yang *et al.* [19] presented a two-branch CNN architecture for rich grain yield estimation so that spectral and spatial features can be separately extracted. The above studies provided evidence regarding the advantages of deep spatial and spectral features over handcrafted features. However, these methods do not take full advantage of spatial–spectral features due to the limitation of 2-D networks.

C. 3-D Convolutional Neural Networks

The 3-D CNN was first proposed for extracting features from spatial and temporal dimensions in human action recognition [43]. Then, the development of the 3-D CNN provided a more effective way to excavate spatial–spectral features. More recently, the 3-D CNN was developed for hyperspectral image (HSI) classification [44], [45]. Instead of extracting spatial and spectral features separately in 2-D networks, the 3-D CNN can capture the joint spatial–spectral features, which is more suitable for 3-D cube data, and has achieved excellent results. For instance, Chen *et al.* [46] proposed a 3-D-CNN-based feature extraction model to extract effective spatial–spectral features of HSI. In this way, the 3-D hypercube with joint spatial–spectral information can be obtained simultaneously. Yang *et al.* [47] proposed a recurrent 3-D CNN method, where the 3-D convolution operator is utilized to exploit both spatial context and spectral correlation through gradually shrinking the patch, and greatly improved performance in HSI classification was achieved. To increase the classification accuracy of HSIs, Mei *et al.* [48] designed a spectral–spatial attention network through spectral and spatial models with 3-D convolution to extract the joint spectral–spatial features. Then, the spectral–spatial attention model was embedded between the above two models to suppress the effects of interfering pixels and capture attention areas in an HSI cube. In [49], a multiscale recurrent neural network (RNN) is presented with spectral–spatial features, where the 3-D CNN is used to extract the local spectral–spatial features and the RNN is used to capture the spatial dependence. The results have proven that the model can capture the deep spectral–spatial features simultaneously, and it outperforms the SAE and 2-D CNN models. The above studies have proven that the 3-D CNN has great superiority in exploiting spatial–spectral features. However, the datasets used in crop yield prediction are different from HSIs, and the process of crop growth is also typical. Therefore, determining how to construct a proper 3-D CNN for predicting yield is a vital problem.

D. Multikernel Learning

Kernel-based methods, such as GPs or SVMs, can model nonlinear data distributions by an implicit mapping function input to the kernel space through kernel embedding [50], [51]. However, in the most general case, a single kernel is not able to fully model the highly complex nonlinear relationship. Hence, a more flexible MKL approach is proposed to address multimodality features by combining multiple kernels. In the multikernel framework, each kernel stands for a certain kind of feature. The fusion of features through multikernels can and has achieved state-of-the-art performance in many fields. For example, Cao *et al.* [52] developed a multikernel-based feature fusion and selection method with a kernel logistic regression model for modeling multiple visual characteristics. To incorporate high-dimensional feature space, Tuia *et al.* [53] proposed a kernel-alignment-based model based on the automatic optimization of the linear combination of kernels, where the weights of each kernel are automatically merged after training the model. Yeh *et al.* [54] presented the MKL framework for fusion of features from different domains. Their method is able to select the class-specific weights for different types of features via the one-versus-rest learning strategy. They then verify the feasibility of their method in feature fusion under MKL. More recently, studies have developed MKL for combining multisource features obtained from different sensors. For example, a new MKL model was proposed to integrate heterogeneous features from LiDAR, and MSI achieved great performance in urban area classification [55]. Later, MKL was also applied for fusion of features from different modalities and yielded improved performance in damage detection. The results revealed the integration of multiple features by MKL led to an additional improvement of approximately 3% [56].

In this work, we aim to explore and integrate hierarchical features for crop yield prediction. Therefore, we first apply a 3-D CNN for excavating deep spatial–spectral features from raw images within a single region. We then incorporate an MKGP to simultaneously capture multiple features through a composite kernel. The experimental results indicate that our method is superior to competing methods with a significant improvement in the wheat yield prediction in China.

III. Methods

A. Problem Setting

In this section, we start by formalizing the crop yield prediction problem. The purpose of crop yield prediction is to predict crop yield before harvest. More specifically, given a set of RSIs $(I^0, I^2, \ldots, I^t)$ from time 0 to t, the model is required to make a reliable prediction yield at time $t+1$. For this article, we are interested in the average crop yield within several counties. Let $\mathrm{X}\,\epsilon\mathcal{R}^{B\times HW}$ denote the $H \times W$ MSI with B bands within each county as the training input, and Y is the crop yield label. Given any new image X^* from the testing set, we aim to predict the probability distribution $P(Y^*|X^*, Y, X)$ of the corresponding crop yield Y^*.

B. Study Area

In this article, we focus on validation our method on winter wheat prediction in China. The main planting areas at county level of wheat are presented in Fig. 1. We further divided the planting areas into three typical types, including the Northern winter wheat part (Zone I), the Southwest winter wheat part (Zone II), and the Xinjiang winter wheat part (Zone III).

C. Overview of the Proposed Approach

Crop yield prediction has been a vital problem, and many studies have been proposed for seeking better performance. In

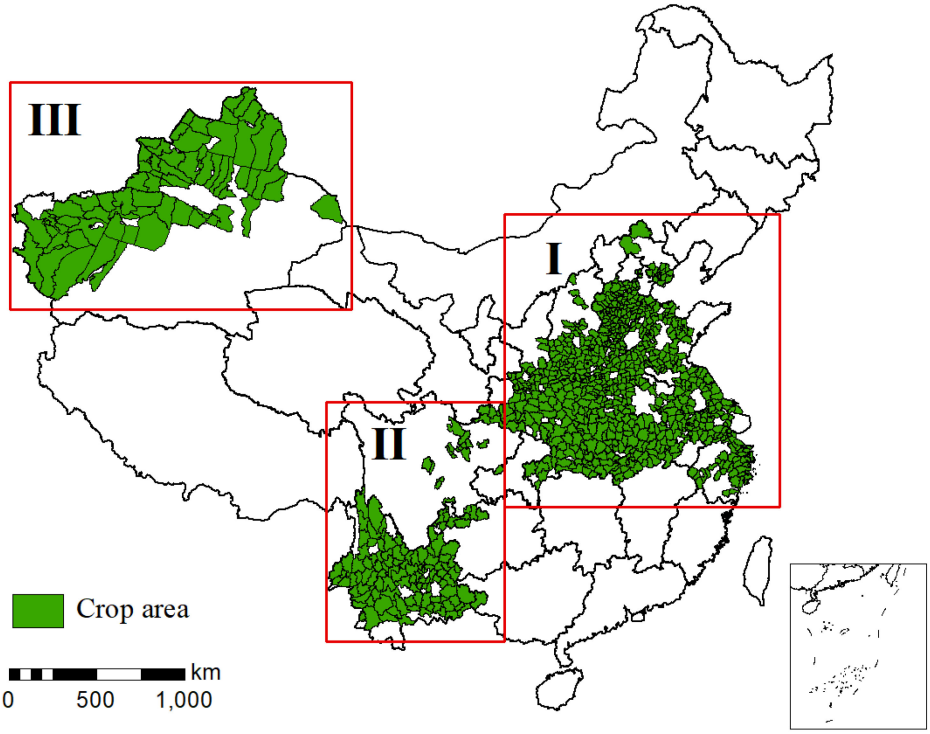

Fig. 1. Winter wheat study area in China.

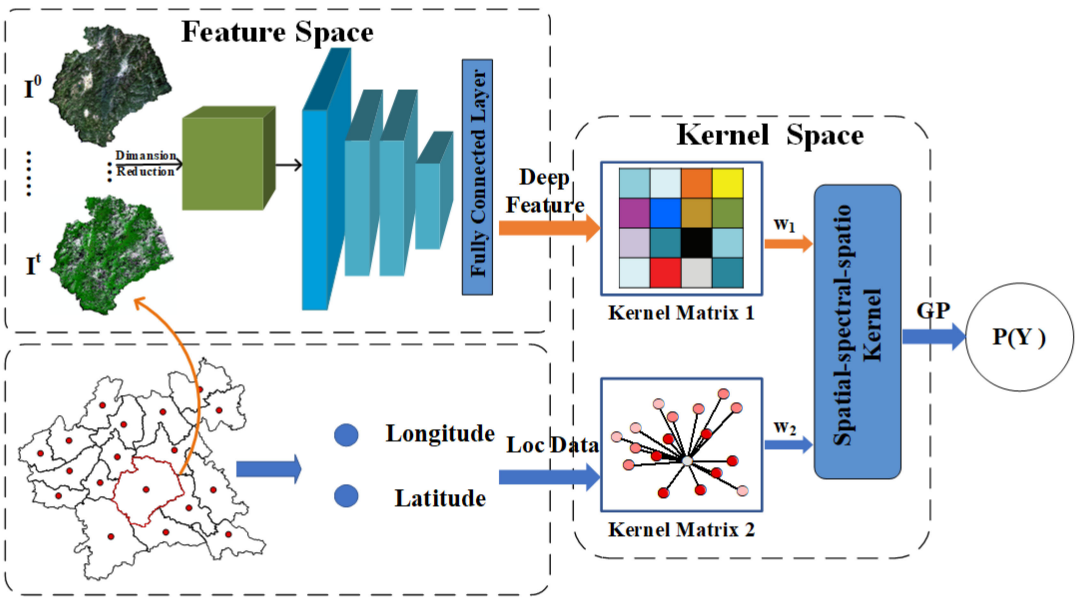

Fig. 2. Architecture of the proposed 3DMKGP.

this study, we focus on exploring and integrating hierarchical features for crop yield prediction.

First, a 3-D CNN is introduced for learning spatial–spectral features from RSIs. In the 3-D CNN, several 3-D convolution kernels are applied for deep feature extraction from MSIs. Second, the prediction process is carried out using an MKGP based on the deep spatial–spectral features and spatial location data. Since the MKGP is capable of systematically aggregating different representations, it can simultaneously capture the deep feature similarities as well as the spatial consistency.

Then, we design a new 3-DMKGP framework by integrating the 3-D CNN and MKGP, as shown in Fig. 2. Two parts are included in our 3-DMKGP: the first part is the feature space, including deep spatial–spectral feature extraction from the 3-D CNN and location data (Loc data) capture. In addition, the MKGP is connected on the top of the 3-D CNN as the kernel space. Finally, the probability distributions of prediction results

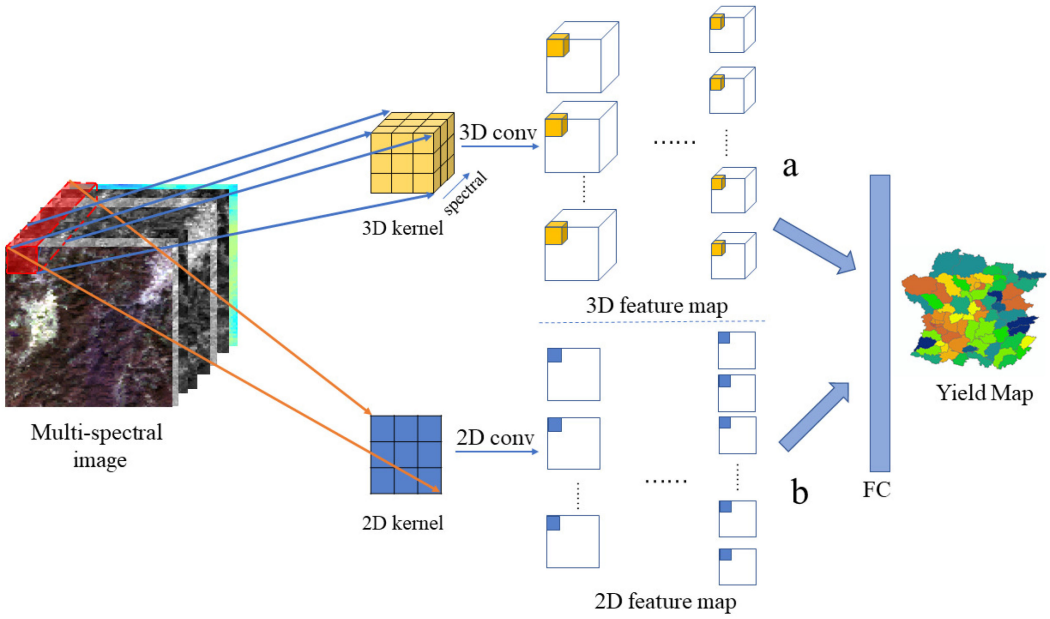

Fig. 3. Difference between (a) 3-D convolution and (b) 2-D convolution on crop yield prediction task.

are established after the kernel space. The proposed 3DMKGP can fully excavate spatial–spectral features from RSIs and make reliable prediction jointly from deep features and location data.

D. 3-D Convolutional Neural Networks

The RSIs used for crop yield prediction in this study are represented by a 3-D cube, which contains a 2-D spatial context and 1-D spectral information. The traditional 2-D CNN uses the 2-D convolution kernels during the process of feature learning and moves in two directions (x, y) to calculate low-dimensional features from the image data. The output shape is also a 2-D matrix, which neglects the spectral information along the third dimension. The 3-D CNN applies 3-D convolution kernels to the dataset, and the convolution kernels move in three directions (x, y, z) to calculate the spatial and spectral feature representations. Most importantly, the output shape after 3-D convolution is a 3-D volume space such as a cube or cuboid, which can jointly learn the spatial and spectral features via different kernels. The difference between 2-D CNNs and 3-D CNNs can be seen from Fig. 3. Hence, in order to fully explore both spatial and spectral discrimination simultaneously, the 3-D CNN is adopted in the proposed method, including 3-D convolution, 3-D pooling, and 3-D batch normalization (BN).

1) 3-D Convolution: As shown in Fig. 3, for an input $I \epsilon \mathcal{R}^3$, the value at position (x, y, z) on the jth feature map in the ith convolution layer is represented as

$$v_{ij}^{xyz} = f\left(b_{ij} + \sum_{m}\sum_{p=0}^{P_i-1}\sum_{q=0}^{Q_i-1}\sum_{r=0}^{R_i-1} w_{ijm}^{pqr} v_{(i-1)m}^{(x+p)(y+q)(z+r)}\right) \tag{1}$$

where f is an activation function and m stands for the number of feature maps in the $(i-1)$th layer (previous layer), and w_{ijm}^{pqr} is the weight at the position (p, q, r) in the 3-D convolution layer that connects to the feature maps of adjacent layers. P_i, Q_i, and R_i are the height, width, and depth of the kernel, respectively, and b_{ij} denotes the bias.

2) 3-D Pooling: Max pooling is used to reduce the number of training parameters of the 3-D CNN in this article. Different from 2-D pooling, 3-D max pooling can perform downsampling by dividing 3-D input into cuboidal pooling regions and computing the maximum of each region. The feature after pooling at position (x, y, z) is defined as

$$O^{x,y,z} = \max_{t} F_t^{x,y,z} \tag{2}$$

where F stands for the features extracted from 3-D convolution kernels before the pooling layer.

3) 3-D Batch Normalization: Assume that X is a mini-batch input; the output of a normalized 3-D batch can be represented as

$$y = \frac{\gamma x}{\sqrt{\text{Var}(x) + \epsilon}} + \left(\beta - \frac{\gamma E(x)}{\sqrt{\text{Var}(x) + \epsilon}}\right) \tag{3}$$

where $E(x)$ and $\text{Var}(x)$, respectively, represent the mean and standard deviation that are calculated over the mini-batch, and γ and β stand for the trainable parameters.

E. Multikernel GP

The kernel space employs a kernel-based method, the GP, by integrating the deep features extracted from the 3-D CNN and the location of the study regions. In this section, we first present a brief introduction about the GP, and then, the MKGP is adopted to integrate the deep features and spatial consistency.

1) Gaussian Process: A GP is a collection of random variables, any finite number of which have a joint Gaussian distribution [57]. Moreover, GP is a nonparametric probability model that is completely specified by the mean and covariance

functions, and the distribution can be denoted as

$$f(x) \sim \text{gp}(m(x), k(x, x')) \tag{4}$$

where x and x' stand for any random variables, the mean function $m(x)$ represents the expectation $E[f(x)]$, and the kernel function $k(x, x')$ defines the covariance $\text{cov}(f(x), f(x'))$.

Usually, for notational simplicity, we will take the mean function to be zero, and furthermore, we add noise $\varepsilon \sim \text{gp}(0, \sigma^2)$ so that the function distribution is closer to the real data.

For the regression problem, we consider

$$y = f(x) + \epsilon. \tag{5}$$

Moreover, we can infer the distribution of the observations y

$$y \sim N(0, K(x, x') + \sigma_n^2 I_n) \tag{6}$$

where I_n is an n-dimensional identity matrix.

Hence, given the input latent variable set $X = \{x_1, x_2, \ldots, x_N\}$, we define the crop yield as $Y = \{y_1, y_2, \ldots, y_N\}$, which is a multivariate GP indexed by x_i; then, we have

$$\begin{aligned} P(Y|X, \theta) &= \prod_{i=1}^{N} p(y_i|x_i, \theta) \\ &= \frac{1}{(2\pi)^{\frac{DN}{2}} |K_Y|^{\frac{D}{2}}} exp\left(-\frac{1}{2} tr\left(K_Y^{-1} y Y^T\right)\right) \end{aligned} \tag{7}$$

where K_Y is an $(n \times n)$-order symmetric positive covariance matrix, and the element in matrix $(K_Y)_{ij} = k_Y(x_i, x_j)$ is used to measure the similarity between x_i and x_j. I_n is an n-dimensional identity matrix.

2) Spatial–Spectral–Spatio Kernel: Based on (7), we can infer that the performance of prediction is dependent on the selection of the kernel function. Hence, in this section, a compound kernel for the GP under the multikernel framework is constructed for capturing hierarchical features. The kernel employed consists of two separate components: deep feature kernel and spatial feature kernel. The weight of each kernel is learned during an optimization phase.

a) Deep spatial–spectral feature kernel: In this part, we intend to model the distance of the deep features extracted from the 3-D CNN. For this purpose, a radial basis function (RBF) kernel is used to build the deep feature kernel based on the spatial–spectral features extracted near the top of the 3-D CNN. Let $X = x_1, x_2, \ldots, x_i$ be the features generated after the 3-D CNN. Then, the feature kernel can be expressed as

$$K_{\text{dfeature}} = \sigma_f^2 \text{exp}\left[-\frac{\|x - x'\|_2^2}{2l_f^2}\right] \tag{8}$$

where x denotes the normalized deep feature of the training dataset, and x' is the feature of the test data. σ_f^2, σ_s^2, l_f, l_l, and l_y are the hyperparameters of this kernel, which are defined as $\theta_1 = \{\theta_l | l = 1, \ldots, M\}$.

b) Spatial consistency feature kernel: For the sake of capturing spatial consistency, we also construct the spatial kernel based on the RBF kernel. The kernel can be expressed as

$$K_{\text{spatial}} = \sigma_s^2 \text{exp}\left[-\frac{\|\Delta_{\text{loc}}\|_2^2}{2l_s^2}\right]. \tag{9}$$

In the spatial kernel, the similarity is measured among the instances of the spatial location of the data points, where $\Delta_{\text{loc}} = |\text{loc} - \text{loc}'|$ represents the distance metric between training and testing data. In this study, we used the central longitude and latitude of each county as the measurement of spatial distance. The hyperparameters in this kernel can be defined as $\theta_2 = \{\theta_l | l = 1, \ldots, K\}$.

c) Spatial–spectral–spatio kernel: To simultaneously aggregate the information within deep features and the spatial consistency, we construct a new "spatial–spectral–spatio" kernel by combining the deep feature kernel and spatial feature kernel using an MKL approach. In this new kernel, we construct two similarity matrices for each data source through the Euclidean distance. The new kernel can be expressed by

$$K = \sum w_s k_s(x_i, x_j) \tag{10}$$

where $W_S = \{w_1, w_2\}$ are the weights of the subkernels. We define the weights positive and $w_1 + w_2 = 1$. The optimized weights w_1 and w_2 are capable of reflecting the contributions of each kind of feature. $K_S = \{K_{\text{dfeature}}, K_{\text{spatial}}\}$ stands for the deep feature kernel and spatial kernel, respectively. As the parameters may be different for different kernels, we define the parameter vector as $\theta_m = \{\theta_1, \theta_2, w_1, w_2\}$ for the new kernel. The detailed parameter settings will be discussed in Section IV.

3) Prediction: Finally, based on the new "spatial–spectral–spatio" kernel, let Y denote the training yield dataset, and y' is the yield that needs to be predicted. The joint distribution of observations Y and predictions y' can be expressed as

$$\begin{bmatrix} Y \\ y' \end{bmatrix} \sim \left(0, \begin{bmatrix} K(X, X) + \sigma_n^2 I_n & K(X, x') \\ K(x', X) & k(x', x') \end{bmatrix}\right) \tag{11}$$

$K(X, x') = K(x', X)^T$ represent the $(n \times 1)$th-order covariance matrix between prediction variables x' and training set X.

Based on the joint distribution (11), we can calculate the probability distributions of prediction yield y':

$$P(y'|x', X, Y) \sim N(E[y'], \text{cov}(y')) \tag{12}$$

where

$$E[y'] = K(x', X)[K(X, X) + \sigma_n^2 I_n]^{-1} y \tag{13}$$

and

$$\begin{aligned} \text{cov}(y') = k(x', x') - K(x', X) \\ \times [K(X, X) + \sigma_n^2 I_n]^{-1} K(X, x'). \end{aligned} \tag{14}$$

Then, we adopt $E[y']$ as the final prediction result. The $\text{cov}(y')$ is used as the measurement of uncertainty.

TABLE I
NUMBER OF TRAINING AND TESTING SAMPLES OF CROP YIELD DATA

	Training	Testing			
		2015	2016	2017	2018
3D CNN	11352	816	765	691	663
MKGP & Traditional	6377	816	765	691	663

IV. EXPERIMENTS

In this section, we examine the superiority of the proposed 3DMKGP for crop yield prediction. Toward this end, several experiments have been conducted.

A. Data Description and Processing

1) Remote Sensing Series: In this article, we focus on the winter wheat yield prediction in China. The remote sensing data used in this article are acquired from the MODIS satellite, including two imagery products. The Surface Reflectance (MOD09A1) dataset [58] contains seven bands that provide rich spectral information. The Land Surface Temperature dataset (MYD11A2) [59] contains two bands that provide the necessary temperature information. Both of them provide eight-day composites. Based on the wheat growth period, only the image taken from the 280th day of the year to the 150th day of the next year are selected. In addition, our study only focuses on the crop area, so the MODIS Annual Land Cover data [60] are used to remove the noncrop pixels. All datasets are acquired from Google Earth Engine [61]. Finally, the remote sensing dataset $(I_1^{(h\times w\times b)}\cdots I_t^{(h\times w\times b)})$ is used for crop yield prediction and includes four dimensions. For such a high-dimensional training labeled data, it will be easy to overfit by training an end-to-end deep network directly based on the original data. To avoid this problem, we employ the same dimension reduction method proposed in [14]. After this, the original 4-D data are transformed into a 3-D histogram $(I^{\text{bins}*\text{time}*\text{bands}})$.

2) Crop Yield Data: County-level wheat yields from 2001 to 2018 were taken from the Agricultural Statistic Yearbook [62] and the Resource Discipline Innovation Platform [63]. All yields are reported in the units of metric tons per kilometer. Furthermore, because the MODIS cropland mask does not distinguish wheat from other crops, we ignored the regions that contributed the bottom 5% of total production in China. Hence, our model is only trained on regions with significant wheat crop cover, and noisy crop yield values are filtered from regions. Finally, a total of 14 287 counties are selected as the final study area. Then, we select the crop data of 2001–2014 as the training dataset. The crop data from 2015 to 2018 are used as the test dataset. Additionally, for the MKGP and traditional algorithms, we did not take the entire time-series data as our test and training dataset because of the calculation limitations. Only the data of 2006–2014 are used as the training data, and the data of 2015–2018 as the test data. The number of the training and testing data samples displayed in Table I.

TABLE II
CONFIGURATIONS OF THE 3-D CNN STRUCTURE

Name	Kernel	Stride	Output Size
Input	-	-	32×32×9
Cov1-1	3×3×3	1	32×32×9×64
Pool1	2×2×2	2	16×16×5×64
Cov2-1	3×3×3	1	16×16×5×128
Pool2	2×2×2	2	8×8×3×128
Cov3-1	3×3×3	1	8×8×3×256
Cov3-2	3×3×3	1	8×8×3×256
Pool3	2×2×2	2	4×4×2×256
FC3	-	-	1024

B. Experiment Setup

1) Implementation Details: The proposed 3DMKGP and other deep learning methods are designed, trained, and tested based on the TensorFlow framework [64]. The parameter settings of the proposed 3-D CNN are listed in Table II. We use Adam as the optimizer and employ dropout after the dense layer to avoid overfitting. The BN technique is also utilized at the end of all convolutional layers to accelerate the convergence and improve the prediction accuracy. Our 3-D CNN is trained with an initial learning rate of 0.003, and weight decay is $1e^{-5}$. A minibatch is set to 20. For hardware system configuration, all the following experiments are completed on a 64-bit Intel Core CPU i7-6900K @ 3.20 GHz with an NVIDIA GeForce 1080 GPU. The RAM memory is 62 GB. Only one GPU is used, under CUDA version 9.0.176.

2) General Information: To validate the effectiveness of the proposed 3DMKGP, it is compared with the most widely used crop yield prediction methods. They are summarized as follows.

1) *SVM [3], [65]:* It is an effective approach for crop yield prediction. Here, an SVM is constructed based on the RBF kernel with the complexity parameter. The degree of the kernel function and the penalty factor C in the SVM are determined by cross validation with the degree varying in the range from 1 to 7, and the C parameter is chosen from the set $10^{-4}, 10^{0}, ..., 10^{6}$.
2) *RF [6], [66]:* It is a supervised ensemble learning algorithm that acts based on decision trees (DTs). A grid search for model performance optimization is carried out with the fivefold cross-validation technique based on the R^2 metric. In this article, we search the number of generated trees from 50 to 500, and we allow a maximum tree depth of 7.
3) *DT [67]:* It is another effective algorithm used for regression with a several leaf nodes. Here, we set the max depth of the trees at 10.
4) *2-D CNN [15]:* It is a widely used deep learning method that has proven to achieve great success in crop yield prediction. The iterations are set up to 50 000. The initial learning rate is 0.003.
5) *LSTM [6], [68]:* It is another widely used deep learning method that has shown promising performance in classification and regression tasks.

TABLE III
ACCURACY COMPARISON OF CROP YIELD PREDICTION AT COUNTY LEVEL

	2015			2016			2017			2018			Avg.		
	RMSE	R^2	MAPE	RMSE	R^2	MAPE	RMSE	R^2	MAPE	RMSE	R^2	MAPE	RMSE	R^2	MAPE
DT-NDVI	1.27	0.44	23.99	1.34	0.38	26.12	1.24	0.46	25.58	1.17	0.44	22.99	1.25	0.43	24.67
RF-NDVI	1.16	0.53	22.31	1.17	0.53	23.16	1.19	0.50	23.64	1.21	0.43	23.33	1.20	0.43	24.22
SVM-NDVI	1.12	0.57	21.46	1.12	0.57	22.83	1.23	0.47	25.18	1.07	0.63	18.06	1.13	0.56	21.88
DT-Hist	1.20	0.51	24.96	1.13	0.56	23.20	1.13	0.55	23.63	1.09	0.51	20.81	1.14	0.53	23.15
RF-Hist	1.10	0.60	22.15	1.12	0.59	20.79	1.05	0.63	20.68	1.03	0.59	18.55	1.08	0.60	20.54
SVM-Hist	1.01	0.66	20.38	1.07	0.63	20.89	1.02	0.66	18.99	0.97	0.63	18.62	1.02	0.64	19.72
LSTM	0.93	0.70	17.70	1.12	0.57	23.14	0.97	0.67	19.06	0.93	0.64	17.34	0.98	0.64	19.31
2D CNN	0.96	0.68	19.51	0.89	0.72	17.53	0.96	0.67	19.70	0.95	0.63	19.49	0.94	0.67	19.05
3DMKGP	**0.76**	**0.79**	**14.68**	**0.71**	**0.82**	**13.88**	**0.73**	**0.81**	**14.87**	**0.73**	**0.78**	**13.98**	**0.73**	**0.80**	**14.35**

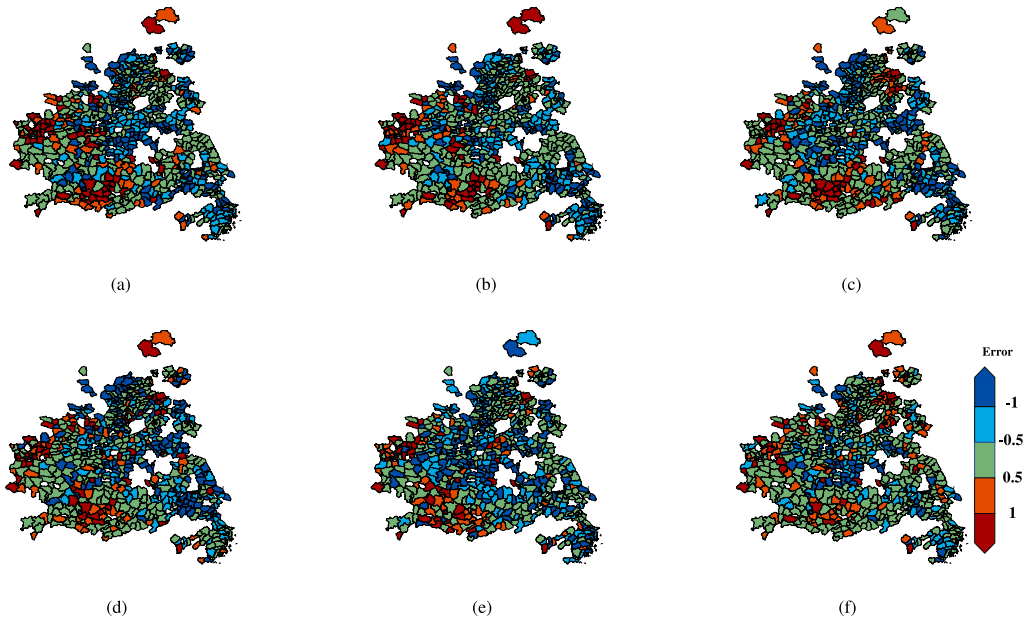

Fig. 4. County-level error maps of Northern winter wheat region. (a) DT. (b) RF. (c) SVM. (d) LSTM. (e) 2-D CNN. (f) 3DMKGP.

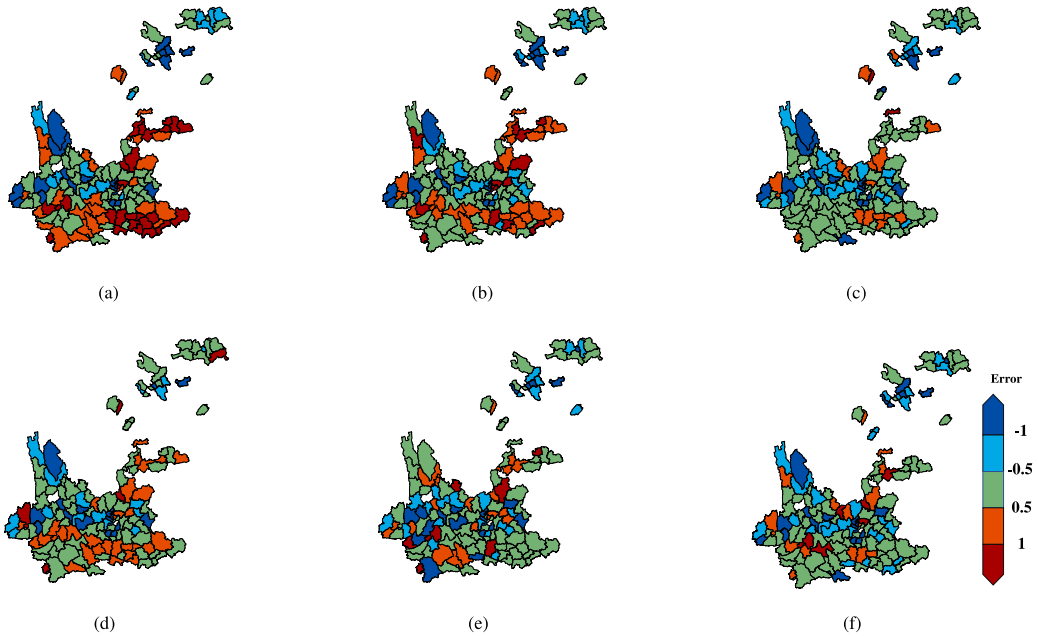

Fig. 5. County-level error maps of Southwest winter wheat region. (a) DT. (b) RF. (c) SVM. (d) LSTM. (e) 2-D CNN. (f) 3DMKGP.

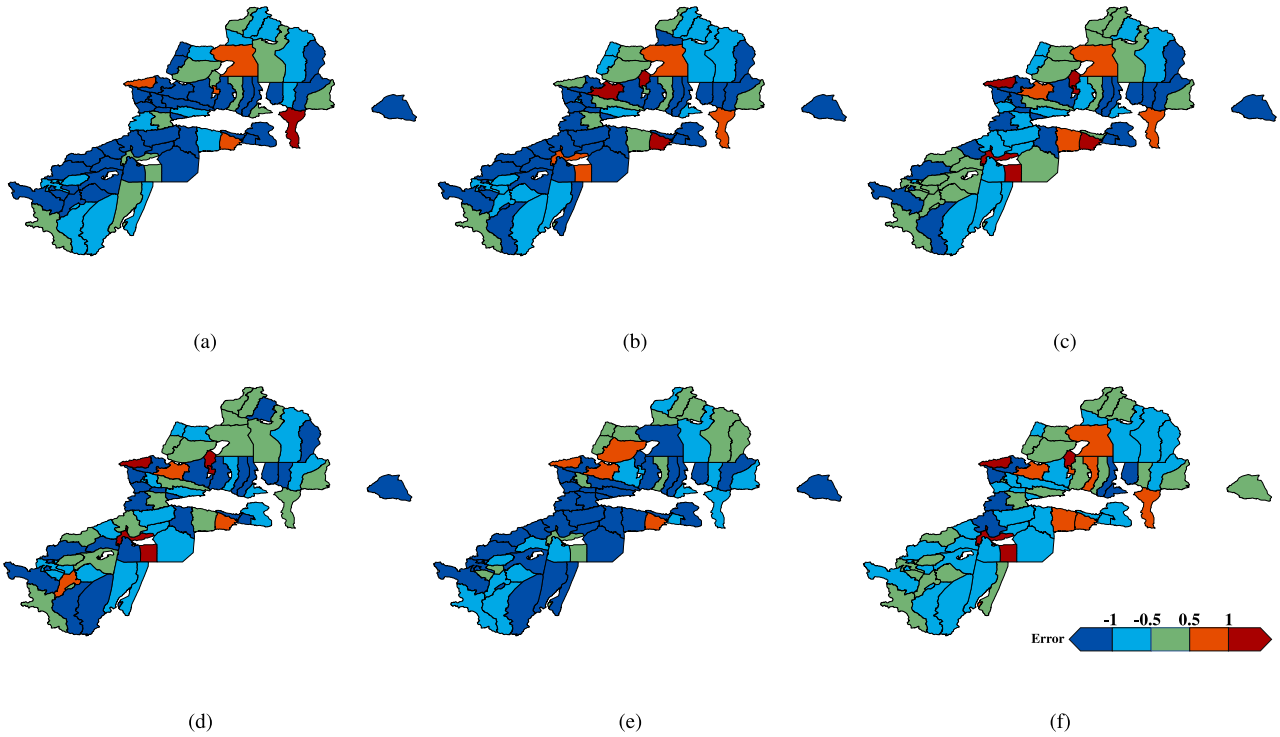

Fig. 6. County-level error maps of Xinjiang winter wheat region. (a) DT. (b) RF. (c) SVM. (d) LSTM. (e) 2-D CNN. (f) 3DMKGP. The error bar represents the difference between prediction and real yield.

TABLE IV
COMPARISON ANALYSIS OF CRUCIAL COMPONENT IN 3DMKGP

	2015			2016			2017			2018			Avg.		
	RMSE	R^2	MAPE	RMSE	R^2	MAPE	RMSE	R^2	MAPE	RMSE	R^2	MAPE	RMSE	R^2	MAPE
LSTMGP	0.95	0.69	18.32	1.00	0.66	19.77	0.94	0.62	18.48	0.88	0.68	16.61	0.94	0.66	18.32
2DGP	0.98	0.66	20.00	0.88	0.73	17.74	0.96	0.68	19.96	0.90	0.67	18.48	0.93	0.68	19.04
3DGP	0.77	0.79	20.61	0.75	0.80	15.54	0.80	0.77	18.02	0.76	0.76	15.21	0.77	0.78	17.34
LSTM-MKGP	0.94	0.69	17.83	0.96	0.68	18.88	0.91	0.71	17.99	0.84	0.70	15.86	0.91	0.69	17.64
2DMKGP	0.86	0.74	16.41	0.81	0.77	15.40	0.83	0.76	15.82	0.83	0.72	15.78	0.83	0.74	15.85
3DSGP	**0.72**	**0.82**	**14.41**	0.74	0.81	13.36	0.77	0.79	17.33	0.76	0.76	13.20	0.75	0.79	14.57
3DMKGP	0.76	0.79	14.68	**0.71**	**0.82**	**13.88**	**0.73**	**0.81**	**14.87**	**0.73**	**0.78**	**13.98**	**0.73**	**0.80**	**14.35**

3) Evaluation Matrix: In this article, in order to evaluate the performance of different crop yield prediction methods, we consider the most common metrics for evaluating regression results, namely, RMSE, R^2, and MAPE, between the ground truth yield and the estimated yield as the evaluation criteria, which can defined as follows:

$$\text{RMSE} = \sqrt{\frac{1}{m}\sum\nolimits_{i=1}^{m}(p_i - y_i)^2} \tag{15}$$

$$R^2 = 1 - \sum_{i=1}^{m}(p_i - y_i)^2 / \sum_{i=1}^{m}(p_i - \overline{y})^2 \tag{16}$$

$$\text{MAPE} = \frac{100\%}{m}\sum_{i=1}^{m}\left|\frac{p_i - y_i}{p_i}\right| \tag{17}$$

where m is the number of predicting data points, y_i and p_i stand for the label and predicting yield, respectively, and $\overline{y}$ denotes the average value of the predicted results.

C. Comparisons With Competing Methods

In this section, we compare the proposed method with three traditional models (SVM, RF, and RT) and two deep learning models (2-D CNN and LSTM) to prove the necessity and advancement of the proposed 3DMKGP in crop yield prediction. In this experiment, the input of deep learning methods is a 3-D histogram with the size of 32 $\times$32$\times$ 9. The performance of traditional models is evaluated on two datasets, including the most widely used handcrafted feature NDVI (DT-NDVI, RF-NDVI, and SVM-NDVI) and the histogram utilized in deep learning methods (DT-Hist, RF-Hist, and SVM-Hist). The NDVI features are extracted from the original RSI of the region of interest during the experimental time series, and the same data processing and dimension reduction method is employed. Therefore, the NDVI images are transformed into a 32$\times$32 NDVI histogram and then flatten into a 1024-D vector as the first input. And the histogram is also transformed into a flatten vector with the size of $32\times32\times9 = 9216$ as the final input. All the hyperparameters

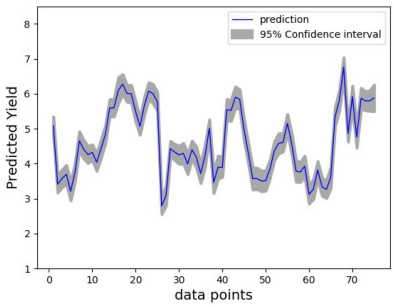

Fig. 7. Uncertainty estimation of prediction results. The shades of gray represent 95% confidence.

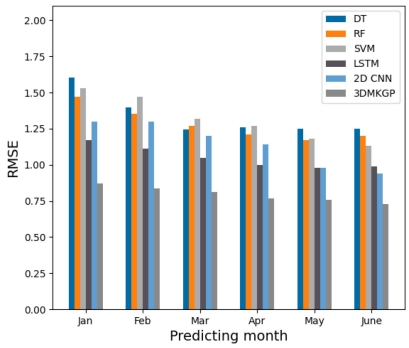

Fig. 8. Experiments of different models with different growth period at county-level prediction.

in traditional machine learning algorithms are determined by fivefold cross validation, and for the hyperparameters θ_m of the new "spatial–spectral–spatio" kernel described in Section III, we first optimized θ_1 and θ_2 within each kernel individually. For σ_f and σ_s, the algorithm searches from 1 to 19. l_f and l_s are searching from 10^{-2} to 10^3. Finally, the weights of each kernel are also optimized between 0 and 1 at 0.1 intervals. The RMSE of all competitors and the proposed method on the crop yield prediction task can be found in Table III.

We first compare the proposed method with traditional methods for a baseline comparison. For the traditional models, the performance of DT-NDVI, RF-NDVI, and SVM-NDVI is inferior to DT-Hist, RF- Hist, and SVM-Hist. This is because the histogram can provide more spectral features compared with the NDVI. However, the proposed 3DMKGP effectively surpasses all traditional models and obtains the best results in all of the testing years. Regarding the traditional methods, the SVM-hist obtained a better performance among them. Compared to the SVM-hist, the decreases in RMSE achieved by 3DMKGP are 0.25, 0.41, 0.29, and 0.24. The improvements in R^2 are 0.13, 0.19, 0.15, and 0.15 for four testing years. These findings proved that our methods have better advantages over traditional models in crop yield prediction. To further verify the superiority of 3DMKGP, we complement various deep learning methods for crop yield prediction. The deep learning methods perform better than the traditional methods. However, our method still surpasses these deep learning methods in all testing years, with the highest R^2 of 0.80 and lowest RMSE and MAPE values of 0.73 and 14.35, respectively. Compared with the LSTM, the 3DMKGP reduced the RMSE by 25.5% and MAPE by 25.7% on average. Compared with the 2-D CNN, the average R^2 of 3DMKGP increased by 19.4% and the RMSE and MAPE decreased by 22.3% and 24.6%, respectively.

To further present the effectiveness of the proposed method, we divided the testing data points into three main parts according to Fig. 1 and visualized the prediction errors of these three wheat producing areas. Corresponding to Table III, similar conclusions can be drawn from the prediction error maps presented in Figs. 4–6, from which it is obvious that the maps provided by the proposed model achieve the lowest error in most counties. Specifically, the regions that are seriously overestimated and underestimated by competing methods are apparently corrected in our 3DMKGP. These results reveal the fact that our 3DMKGP model can construct a more powerful crop-related representation. The first reason is that the 3-D CNN in the 3DMKGP can make full use of both spatial and spectral information from MSIs. Second, the new "spatial–spectral–spatio" kernel makes it possible for the 3DMKGP to simultaneously capture deep features and spatial correlation and automatically adjust the weight of each feature, which enables 3DMKGP with better suitability for crop yield prediction.

D. Analysis of the Proposed Method: Effect of Different Components

In this section, based on above explanation, extensive experiments are conducted to verify the effectiveness of the crucial components in 3DMKGP. Here, we analyze the superiority of the 3-D CNN in extracting spatial–spectral features, and then, we compare the effect of the MKGP strategy. These experiments demonstrate different contributions of components and provide more insights of our proposed method.

1) 3-D CNN Component: We first evaluated the effectiveness of the 3-D CNN in our framework. For this purpose, we replace the 3-D CNN component in the proposed framework with different 2-D networks, including 2-D CNN and LSTM (CNN-MKGP and LSTM-MKGP). The experimental results shown in Table IV clearly demonstrate that 3DMKGP outperforms CNN-MKGP and LSTM-MKGP in all testing years and achieves a lower RMSE of 0.1 and 0.18, respectively. CNN-MKGP has slightly improved compared with LSTM-MKGP; however, it also leads to unsatisfactory performance because they do not fully exploit the spatial–spectral features. Compared to the CNN-MKGP, the 3DMKGP obtains 8% gains in R^2. Due to the clear improvement of the 3DMKGP, it can be confirmed that the 3-D convolutions make it possible to fully use spatial–spectral information.

2) MKGP Component: In this experiment, we investigate the effectiveness of the designed MKGP. For this purpose, we first constructed a single-kernel GP, where the kernel is structured with the deep features extracted from LSTM, 2-D CNN, and 3-D CNN (LSTMGP, 2DGP, and 3DGP). Then, we compared them with our MKGP that is also implemented on three different deep learning networks (LSTMKGP, 2DMKGP, and 3DMKGP). Moreover, since the GP is also utilized for incorporating the spatial dependency in [14]. We further implement the experiment to compare our multi-kernel GP with their single-GP strategy.

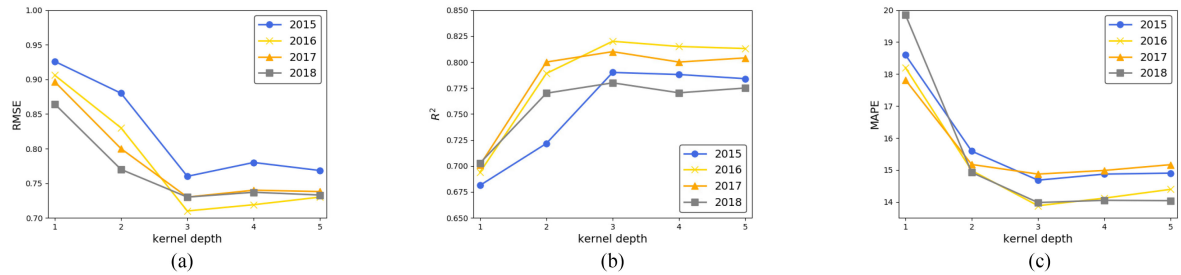

Fig. 9. Evaluation performance of different kernel depth in terms of (a) RMSE, (b) R^2, and (c) MAPE.

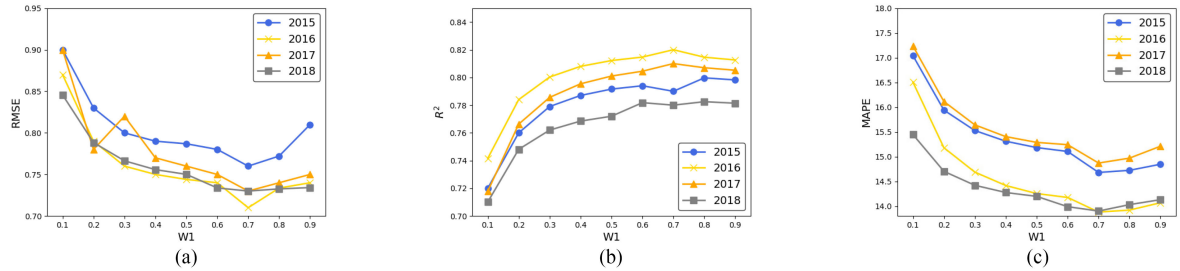

Fig. 10. Evaluation performance of different feature weights in terms of (a) RMSE, (b) R^2, and (c) MAPE; w_1 stands for the weight of spatial–spectral feature kernel.

Especially, we have changed the deep network of [14] with our proposed 3-D CNN (3DSGP) to avoid the influence of network structure. The comparison results are shown in Table IV.

It is noticed that the results obtained by the MKGP by integrating all features are always superior in all testing years. In greater detail, the RMSE provided by the MKGP with the 3-D CNN, 2-D CNN, and LSTM are 0.04, 0.10, and 0.03 lower than that of the DGP in RMSE, respectively. The MKGP improves on the performance of the DGP and obtains 0.02, 0.06, and 0.03 gains in R^2. Hence, it can be concluded that by modeling the long-term dependencies in the spatial dimension, it can provide a higher performance for crop yield prediction. These results demonstrate that our MKGP better exploits the hierarchical features and is more effective than a single feature for the crop yield prediction. Besides, comparing with the 3DSGP, our method obtains a better result in three of the four testing years. This further improve the effectiveness of the proposed MKGP.

3) Uncertainty Estimation: In real-world applications, one of the key points of the prediction problem is offering the uncertainty of the results. The 3DMKGP can learn a probability distribution of the predictions, which provides a natural way for uncertainty estimation. In this part, the 95% prediction intervals that are calculated from the 3DMKGP based on (14) have been used to estimate the random error in the crop yield prediction. Fig. 7 illustrates the predictions and corresponding uncertainty obtained from 3DMKGP.

E. Crop Yield Prediction Before Harvest

The ultimate goal of crop yield prediction is predicting the crop yield before harvest. To this end, we train and test our model based on different time windows. The starting of windows is triggered by the sowing period (October), and the ending point is varying from February to June (harvest) of the following year. Fig. 8 shows the averaged RMSE in different time windows. It can be observed that with the ending point closer to the sowing month, the performance of all models gradually improved. All the other models except 3DMKGP did not perform well in the early months since the information in the early months is not obvious. Moreover, our proposed method 3DMKGP outperforms other methods consistently at all time windows, demonstrating the robustness of the proposed method. Besides, it is noticed that the RMSE remains steady after May in the proposed method, suggesting that our method can predict the crop yield two months before harvest.

F. Parameter and Feature Analysis

1) Experiments With Different Kernel Depths: One of the contributions in this study is that the 3-D CNN is applied to explicitly spatial–spectral features. Different from the 2-D CNN, the third dimension of 3-D convolution layers can explore the spectral correlation through the 3-D kernel. To explore the influence of the kernel size, we vary the kernel depth while keeping all other common settings fixed. Here, we experiment with different kernel depths that are set from 1 to 5. Note that depth $= 1$ has the same architecture as the 2-D CNN. The experimental results of the 3-D CNN with different kernel spectral depths are shown in Fig. 9. It is observed that depth $= 3$ achieves the best results among all the kernels. As expected, depth $= 1$ has the worst results since it is equal to a 2-D CNN that cannot fully excavate spatial–spectral features.

2) Experiments With Different Weights of Hierarchical Features: The new "spatial–spectral–spatio" kernel is the combination of two kernels, and the optimized weights of each kernel will directly give a ranked importance to each kind of feature.

To show that each feature has contributed to the overall result, we highlight the contribution of the deep spatial–spectral feature and the spatial consistency feature by adjusting the weight of the deep feature kernel w_1 in (10). From Fig. 10, we can see that the optimized weights with $w_1 = 0.7$ and $w_2 = 0.3$ achieve the best performance, which indicates that deep features play a dominant role in predicting crop yield. With the value of w_1 decreasing, the RMSE tends to continuously increase. Additionally, the spatial consistency feature also plays an important role in predicting crop yield with a weight of 0.3. The analysis of w_i can help illustrate each feature's contribution and provide more insight for feature selection in crop yield prediction.

V. Conclusion

In this article, an effective model is proposed that involves hierarchical features for crop yield prediction. We first utilize the superiority of the 3-D CNN that enables extracting spatial–spectral features from raw RSIs. To further account for the features beyond the RSIs, we employ an MKL framework that fuses these deep features with spatial consistency features between data points. Moreover, the prediction process is implemented in the kernel-based GP method.

County-level winter wheat in China is predicted in this article. Extensive experimental results demonstrate that our method not only outperforms other traditional and deep learning methods but also extracts more discriminative feature representations, which demonstrates its potential application in different prediction problems. In terms of further research, we can fuse more crop-related features with the multikernel approach. Furthermore, our method can be generalized for yield prediction of other crop types.

Acknowledgment

The authors would like to thank the 13th Five-Year Informatization Plan of the Chinese Academy of Sciences (Grant XXH13505-07) for making the crop yield data available.

References

[1] K. Dzotsi, B. Basso, and J. Jones, "Development, uncertainty and sensitivity analysis of the simple SALUS crop model in DSSAT," *Ecol. Model.*, vol. 260, pp. 62–76, 2013.

[2] R. Srinivasan, X. Zhang, and J. Arnold, "SWAT ungauged: Hydrological budget and crop yield predictions in the Upper Mississippi River Basin," *Trans. ASABE*, vol. 53, no. 5, pp. 1533–1546, 2010.

[3] H. Aghighi, M. Azadbakht, D. Ashourloo, H. S. Shahrabi, and S. Radiom, "Machine learning regression techniques for the silage maize yield prediction using time-series images of Landsat 8 OLI," *IEEE J. Sel. Topics Appl. Earth Observ. Remote Sens.*, vol. 11, no. 12, pp. 4563–4577, Dec. 2018.

[4] N. Gandhi, L. J. Armstrong, O. Petkar, and A. K. Tripathy, "Rice crop yield prediction in India using support vector machines," in *Proc. 13th Int. Joint Conf. Comput. Sci. Softw. Eng.*, 2016, pp. 1–5.

[5] U. Saeed, J. Dempewolf, I. Becker-Reshef, A. Khan, A. Ahmad, and S. A. Wajid, "Forecasting wheat yield from weather data and MODIS NDVI using random forests for Punjab Province, Pakistan," *Int. J. Remote Sens.*, vol. 38, no. 17, pp. 4831–4854, 2017.

[6] J. Cao *et al.*, "Integrating multi-source data for rice yield prediction across China using machine learning and deep learning approaches," *Agricultural Forest Meteorol.*, vol. 297, 2021, Art. no. 108275.

[7] M. Kaul, R. L. Hill, and C. Walthall, "Artificial neural networks for corn and soybean yield prediction," *Agricultural Syst.*, vol. 85, no. 1, pp. 1–18, 2005.

[8] B. Ji, Y. Sun, S. Yang, and J. Wan, "Artificial neural networks for rice yield prediction in mountainous regions," *J. Agricultural Sci.*, vol. 145, no. 3, pp. 249–261, 2007.

[9] P. Bose, N. K. Kasabov, L. Bruzzone, and R. N. Hartono, "Spiking neural networks for crop yield estimation based on spatiotemporal analysis of image time series," *IEEE Trans. Geosci. Remote Sens.*, vol. 54, no. 11, pp. 6563–6573, Nov. 2016.

[10] G. Cheng and J. Han, "A survey on object detection in optical remote sensing images," *ISPRS J. Photogrammetry Remote Sens.*, vol. 117, pp. 11–28, 2016.

[11] O. A. Penatti, K. Nogueira, and J. A. Dos Santos, "Do deep features generalize from everyday objects to remote sensing and aerial scenes domains?," in *Proc. IEEE Conf. Comput. Vis. Pattern Recognit. Workshops*, 2015, pp. 44–51.

[12] C. Chen *et al.*, "Exploiting spatio-temporal correlations with multiple 3D convolutional neural networks for citywide vehicle flow prediction," in *Proc. IEEE Int. Conf. Data Mining*, 2018, pp. 893–898.

[13] J.-W. Ma, C.-H. Nguyen, K. Lee, and J. Heo, "Regional-scale rice-yield estimation using stacked auto-encoder with climatic and MODIS data: A case study of South Korea," *Int. J. Remote Sens.*, vol. 40, no. 1, pp. 51–71, 2019.

[14] J. You, X. Li, M. Low, D. Lobell, and S. Ermon, "Deep Gaussian process for crop yield prediction based on remote sensing data," in *Proc. 31st AAAI Conf. Artif. Intell.*, 2017, pp. 4559–4565.

[15] P. Nevavuori, N. Narra, and T. Lipping, "Crop yield prediction with deep convolutional neural networks," *Comput. Electron. Agriculture*, vol. 163, 2019, Art. no. 104859.

[16] A. Kaneko *et al.*, "Deep learning for crop yield prediction in Africa," in *Proc. ICML Workshop Art. Intell. Soc. Good*, 2019.

[17] A. X. Wang, C. Tran, N. Desai, D. Lobell, and S. Ermon, "Deep transfer learning for crop yield prediction with remote sensing data," in *Proc. 1st ACM SIGCAS Conf. Comput. Sustain. Soc.*, 2018, pp. 1–5.

[18] J. Gu *et al.*, "Recent advances in convolutional neural networks," *Pattern Recognit.*, vol. 77, pp. 354–377, 2018.

[19] Q. Yang, L. Shi, J. Han, Y. Zha, and P. Zhu, "Deep convolutional neural networks for rice grain yield estimation at the ripening stage using UAV-based remotely sensed images," *Field Crops Res.*, vol. 235, pp. 142–153, 2019.

[20] A. Haghighattalab, J. Crain, S. Mondal, J. Rutkoski, R. P. Singh, and J. Poland, "Application of geographically weighted regression to improve grain yield prediction from unmanned aerial system imagery," *Crop Sci.*, vol. 57, no. 5, pp. 2478–2489, 2017.

[21] M. Maimaitijiang, V. Sagan, P. Sidike, S. Hartling, F. Esposito, and F. B. Fritschi, "Soybean yield prediction from UAV using multimodal data fusion and deep learning," *Remote Sens. Environ.*, vol. 237, 2020, Art. no. 111599.

[22] L. Anselin, R. Bongiovanni, and J. Lowenberg-DeBoer, "A spatial econometric approach to the economics of site-specific nitrogen management in corn production," *Amer. J. Agricultural Econ.*, vol. 86, no. 3, pp. 675–687, 2004.

[23] N. R. Peralta, Y. Assefa, J. Du, C. J. Barden, and I. A. Ciampitti, "Mid-season high-resolution satellite imagery for forecasting site-specific corn yield," *Remote Sens.*, vol. 8, no. 10, 2016, Art. no. 848.

[24] Y.-S. Shiu and Y.-C. Chuang, "Yield estimation of paddy rice based on satellite imagery: Comparison of global and local regression models," *Remote Sens.*, vol. 11, no. 2, 2019, Art. no. 111.

[25] H. Russello, "Convolutional neural networks for crop yield prediction using satellite images," Master's thesis, Dept. Artif. Intell., Univ. Amsterdam, Amsterdam, The Netherlands, 2018.

[26] P. Nevavuori, N. Narra, P. Linna, and T. Lipping, "Crop yield prediction using multitemporal UAV data and spatio-temporal deep learning models," *Remote Sens.*, vol. 12, no. 23, 2020, Art. no. 4000.

[27] M. Abedinpour, A. Sarangi, T. Rajput, M. Singh, H. Pathak, and T. Ahmad, "Performance evaluation of aquacrop model for maize crop in a semi-arid environment," *Agricultural Water Manage.*, vol. 110, pp. 55–66, 2012.

[28] C. M. T. Soler, P. C. Sentelhas, and G. Hoogenboom, "Application of the CSM-CERES-maize model for planting date evaluation and yield forecasting for maize grown off-season in a subtropical environment," *Eur. J. Agronomy*, vol. 27, nos. 2–4, pp. 165–177, 2007.

[29] B. A. Keating *et al.* "An overview of APSIM, a model designed for farming systems simulation," *Eur. J. Agronomy*, vol. 18, nos. 3/4, pp. 267–288, 2003.

[30] D. K. Bolton and M. A. Friedl, "Forecasting crop yield using remotely sensed vegetation indices and crop phenology metrics," *Agricultural Forest Meteorol.*, vol. 173, pp. 74–84, 2013.

[31] F. A. Vega, F. C. Ramirez, M. P. Saiz, and F. O. Rosúa, "Multi-temporal imaging using an unmanned aerial vehicle for monitoring a sunflower crop," *Biosyst. Eng.*, vol. 132, pp. 19–27, 2015.
[32] G. Ruß and R. Kruse, "Feature selection for wheat yield prediction," in *Research and Development in Intelligent Systems XXVI*. Berlin, Germany: Springer, 2010, pp. 465–478.
[33] J. Frausto-Solis, A. Gonzalez-Sanchez, and M. Larre, "A new method for optimal cropping pattern," in *Proc. Mex. Int. Conf. Artif. Intell.*, 2009, pp. 566–577.
[34] M. Zaefizadeh, A. Jalili, M. Khayatnezhad, R. Gholamin, and T. Mokhtari, "Comparison of multiple linear regressions (MLR) and artificial neural network (ANN) in predicting the yield using its components in the hulless barley," *Adv. Environ. Biol.*, vol. 5, pp. 109–114, 2011.
[35] X. Zhou *et al.*, "Predicting grain yield in rice using multi-temporal vegetation indices from UAV-based multispectral and digital imagery," *ISPRS J. Photogrammetry Remote Sens.*, vol. 130, pp. 246–255, 2017.
[36] J. Xue and B. Su, "Significant remote sensing vegetation indices: A review of developments and applications," *J. Sens.*, vol. 2017, 2017, Art. no. 1353691.
[37] W. Zhou, D. Ming, X. Lv, K. Zhou, H. Bao, and Z. Hong, "SO-CNN based urban functional zone fine division with VHR remote sensing image," *Remote Sens. Environ.*, vol. 236, 2020, Art. no. 111458.
[38] P. Li *et al.*, "Object extraction from very high-resolution images using a convolutional neural network based on a noisy large-scale dataset," *IEEE Access*, vol. 7, pp. 122 784–122795, 2019.
[39] N. Kussul, M. Lavreniuk, S. Skakun, and A. Shelestov, "Deep learning classification of land cover and crop types using remote sensing data," *IEEE Geosci. Remote Sens. Lett.*, vol. 14, no. 5, pp. 778–782, May 2017.
[40] C. Zhang *et al.*, "Joint deep learning for land cover and land use classification," *Remote Sens. Environ.*, vol. 221, pp. 173–187, 2019.
[41] A. Peerlinck, J. Sheppard, and B. Maxwell, "Using deep learning in yield and protein prediction of winter wheat based on fertilization prescriptions in precision agriculture," in *Proc. 14th Int. Conf. Precis. Agriculture*, 2018, pp. 1–13.
[42] S. Khaki and L. Wang, "Crop yield prediction using deep neural networks," *Frontiers Plant Sci.*, vol. 10, 2019, Art. no. 621.
[43] S. Ji, W. Xu, M. Yang, and K. Yu, "3D convolutional neural networks for human action recognition," *IEEE Trans. Pattern Anal. Mach. Intell.*, vol. 35, no. 1, pp. 221–231, Jan. 2013.
[44] S. Mei, J. Ji, Y. Geng, Z. Zhang, X. Li, and Q. Du, "Unsupervised spatial-spectral feature learning by 3D convolutional autoencoder for hyperspectral classification," *IEEE Trans. Geosci. Remote Sens.*, vol. 57, no. 9, pp. 6808–6820, Sep. 2019.
[45] F. I. Alam, J. Zhou, A. W. Liew, X. Jia, J. Chanussot, and Y. Gao, "Conditional random field and deep feature learning for hyperspectral image classification," *IEEE Trans. Geosci. Remote Sens.*, vol. 57, no. 3, pp. 1612–1628, Mar. 2019.
[46] Y. Chen, H. Jiang, C. Li, X. Jia, and P. Ghamisi, "Deep feature extraction and classification of hyperspectral images based on convolutional neural networks," *IEEE Trans. Geosci. Remote Sens.*, vol. 54, no. 10, pp. 6232–6251, Oct. 2016.
[47] X. Yang, Y. Ye, X. Li, R. Y. Lau, X. Zhang, and X. Huang, "Hyperspectral image classification with deep learning models," *IEEE Trans. Geosci. Remote Sens.*, vol. 56, no. 9, pp. 5408–5423, Sep. 2018.
[48] X. Mei *et al.*, "Spectral-spatial attention networks for hyperspectral image classification," *Remote Sens.*, vol. 11, no. 8, 2019, Art. no. 963.
[49] C. Shi and C.-M. Pun, "Multi-scale hierarchical recurrent neural networks for hyperspectral image classification," *Neurocomputing*, vol. 294, pp. 82–93, 2018.
[50] N. D. Lawrence, "Gaussian process latent variable models for visualisation of high dimensional data," in *Proc. Int. Conf. Neural Inf. Process. Syst.*, 2004, pp. 329–336.
[51] B. Gu, V. S. Sheng, Z. Wang, D. Ho, S. Osman, and S. Li, "Incremental learning for ν-support vector regression," *Neural Netw.*, vol. 67, pp. 140–150, 2015.
[52] P. Cao *et al.*, "A multi-kernel based framework for heterogeneous feature selection and over-sampling for computer-aided detection of pulmonary nodules," *Pattern Recognit.*, vol. 64, pp. 327–346, 2017.
[53] D. Tuia, G. Camps-Valls, G. Matasci, and M. Kanevski, "Learning relevant image features with multiple-kernel classification," *IEEE Trans. Geosci. Remote Sens.*, vol. 48, no. 10, pp. 3780–3791, Oct. 2010.
[54] Y.-R. Yeh, T.-C. Lin, Y.-Y. Chung, and Y.-C. F. Wang, "A novel multiple kernel learning framework for heterogeneous feature fusion and variable selection," *IEEE Trans. Multimedia*, vol. 14, no. 3, pp. 563–574, Jun. 2012.
[55] Y. Gu, Q. Wang, X. Jia, and J. A. Benediktsson, "A novel MKL model of integrating LiDAR data and MSI for urban area classification," *IEEE Trans. Geosci. Remote Sens.*, vol. 53, no. 10, pp. 5312–5326, Oct. 2015.
[56] A. Vetrivel, M. Gerke, N. Kerle, F. Nex, and G. Vosselman, "Disaster damage detection through synergistic use of deep learning and 3D point cloud features derived from very high resolution oblique aerial images, and multiple-kernel-learning," *ISPRS J. Photogrammetry Remote Sens.*, vol. 140, pp. 45–59, 2018.
[57] C. E. Rasmussen, "Gaussian processes in machine learning," in *Summer School Machine Learning*. Berlin, Germany: Springer, 2003, pp. 63–71.
[58] E. Vermote, "MOD09A1 MODIS/Terra Surface Reflectance 8-Day L3 Global 500 m SIN Grid v006," *NASA EOSDIS Land Processes DAAC*, vol. 10, 2015.
[59] Z. Wan, S. Hook, and G. Hulley, "MYD11A2 MODIS/aqua Land Surface Temperature and the Emissivity 8-Day L3 Global 1 km SIN Grid," NASA EOSDIS Land Processes DAAC, 2015.
[60] M. Friedl and D. Sulla-Menashe, "MCD12Q1 MODIS/Terra Aqua Land Cover Type Yearly L3 Global 500 m SIN Grid v006 [*data set*]," *NASA EOSDIS Land Processes DAAC*, vol. 10, 2015.
[61] N. Gorelick, M. Hancher, M. Dixon, S. Ilyushchenko, D. Thau, and R. Moore, "Google Earth engine: Planetary-scale geospatial analysis for everyone," *Remote Sens. Environ.*, vol. 202, pp. 18–27, 2017.
[62] National Bureau of Statistics of China, *China Rural Statistical Yearbook*, [EB/OL]. Accessed: Apr. 4, 2010. [Online]. Available: http://www.stats.gov.cn/
[63] Chinese Academy of Sciences, *Resource Discipline Innovation Platform*, [EB/OL]. Accessed: Apr. 4, 2010. [Online]. Available: http://www.data.ac.cn/server/database.html
[64] M. Abadi *et al.*, "Tensorflow: A system for large-scale machine learning," in *Proc. 12th Symp. Oper. Syst. Des. Implementation* , 2016, pp. 265–283.
[65] Y. Cai *et al.*, "Integrating satellite and climate data to predict wheat yield in Australia using machine learning approaches," *Agricultural Forest Meteorol.*, vol. 274, pp. 144–159, 2019.
[66] D. Gómez, P. Salvador, J. Sanz, and J. L. Casanova, "Potato yield prediction using machine learning techniques and Sentinel 2 data," *Remote Sens.*, vol. 11, no. 15, 2019, Art. no. 1745.
[67] J. Han *et al.*, "Prediction of winter wheat yield based on multi-source data and machine learning in China," *Remote Sens.*, vol. 12, no. 2, 2020, Art. no. 236.
[68] R. A. Schwalbert, T. Amado, G. Corassa, L. P. Pott, P. V. Prasad, and I. A. Ciampitti, "Satellite-based soybean yield forecast: Integrating machine learning and weather data for improving crop yield prediction in Southern Brazil," *Agricultural Forest Meteorol.*, vol. 284, 2020, Art. no. 107886.

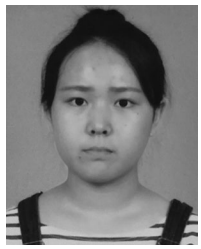

Mengjia Qiao received the B.S. degree in geographic information science from the North China University of Water Resources and Electric Power, Zhengzhou, China, in 2017. She is currently working toward the Ph.D. degree in software engineering with Zhengzhou University, Zhengzhou.

Her research interests include deep learning, remote sensing image classification, regression, and applications.

Xiaohui He was born Shangqiu, China, in 1978. She received the B.E. degree in land resources management from Henan Agricultural University, Zhengzhou, China, in 2000, the M.E. degree in soil science from Northwest A&F University, Xianyang, China, in 2003, and the Ph.D. degree in soil science from the Research Centre of Soil and Water Conservation, Xi'an, China, in 2006.

She visited the University of Kiel, Kiel, Germany, in 2014. She is currently an Assistant Professor with the Institute of Smart City, Zhengzhou University, Zhengzhou. Her research interests include remote sensing big data processing, machine learning, data mining, and artificial intelligence.

Xijie Cheng is working toward the master's degree with the Industrial Technology Research Institute, Zhengzhou University, Zhengzhou, China.

Her research interests include high-spatial-resolution remote sensing classification based on machine learning and deep learning.

Panle Li was born Luoyang, China, in 1992. He received the B.S. degree in information and computing science from the Henan University of Science and Technology, Luoyang, China, in 2015, and the M.S. degree in software engineering in 2015 from Zhengzhou University, Zhengzhou, China, where he is currently working toward the Ph.D. degree.

His research interests include remote-sensing image processing and analysis and information extraction from high-spatial-resolution satellite remote sensing images.

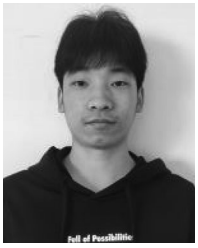

Haotian Luo is working toward the master's degree with the School of the Geoscience and Technology, Zhengzhou University, Zhengzhou, China.

His research interests include high-spatial-resolution remote sensing classification.

Zhihui Tian was born in Xixia, China, in June 1965. He received the Ph.D. degree in geographical information system from Wuhan University, Wuhan, China, in 2006.

He is currently a Professor with the School of the Geoscience and Technology, Zhengzhou University, Zhengzhou, China. His research interests include smart city engineering and high-performance geographic computing.

Hengliang Guo was born in Shangqiu, China, in 1971. He received the M.E. degree in physical geography from South China Normal University, Guangdong, China, in 2001.

He is currently an Associate Professor with the School of the Geoscience and Technology and the Deputy Director of the Henan Supercomputing Center of Zhengzhou University, Zhengzhou, China. His research interests include computer graphics and geospatial visualization and analysis.